Peer-review status: Under review (ERL)

Flooded Rivers, Drying Wetlands, Vanishing Tributaries: Hydrological Paradox of the East Ganga Plains

Manudeo Singh[a]* and S. K. Tandon[b]

[a] Department of Geography and Earth Sciences, Aberystwyth University, Wales, UK

[b] Department of Earth Sciences, Indian Institute of Technology Gandhinagar, India

Corresponding author: manudeo.singh@aber.ac.uk

Flooded Rivers, Drying Wetlands, Vanishing Tributaries: Hydrological Paradox of the East Ganga Plains

Manudeo Singh[a]* and S. K. Tandon[b]

[a] Department of Geography and Earth Sciences, Aberystwyth University, Wales, UK

[b] Department of Earth Sciences, Indian Institute of Technology Gandhinagar, India

*Corresponding author: manudeo.singh@aber.ac.uk

Abstract

The East Ganga Plains (EGP) present a striking hydrological paradox: while embanked rivers flood with increasing magnitude, adjacent wetlands and groundwater-fed streams are desiccating, and aquifer storage is declining. Using satellite remote sensing and gravimetry, we document that: (i) wetlands exhibit significant water-cover loss despite stable monsoon rainfall; (ii) small rivers and tributaries are seasonally desiccating; (iii) vegetation greenness has increased significantly, reflecting irrigation intensification rather than wetter conditions; (iv) GLDAS Noah component separation confirms that 91.8% of the variance in GRACE terrestrial water storage is attributable to groundwater storage change (ΔGW), validating satellite gravimetry as a groundwater proxy and documenting a sustained negative ΔGW anomaly; and (v) Height Above Nearest Drainage (HAND) analysis of trajectory-classified wetland pixels reveals a median elevation of 0.00 m above nearest drainage, with almost three-quarters within 0.25 m, demonstrating that desiccation is embankment-imposed rather than topographically determined. All three cross-variable Pearson correlations between ΔGW, wetness index (MNDWI), and vegetation index (NDVI) ($n = 20$) are significant at $p \leq 0.004$ and fall in the direction predicted by connectivity loss, indicating that irrigation intensification is drawing down aquifer storage and eliminating wetland water cover. The ΔGW–MNDWI coupling is concentrated in the lowest-lying wetland pixels, consistent with direct surface connectivity as the primary mechanism. The Kosi–Gandak interfan provides the most spatially coherent expression of this paradox. This study presents the first basin-scale, multi-proxy synthesis with explicit GLDAS-based groundwater validation for the EGP. We propose a monitoring framework and four research priorities to support hydrologically secure development in this densely populated, underrepresented region.

Keywords: East Ganga Plains; hydrological connectivity; embankments; floodplain wetlands; GRACE groundwater storage; Height Above Nearest Drainage; irrigation-driven greening

1. Introduction

The Ganga Plains support more than 400 million people and are simultaneously a hotspot for both flooding and water scarcity (Brakenridge et al., 2024; Sharma et al., 2025; Chuphal et al., 2025). The Indus–Ganga Plain (IGP) is among the most intensively studied regions in global hydrology, particularly regarding groundwater depletion (Rodell et al., 2009), surface-water change (Nagel et al., 2025), and irrigation-driven land-cover dynamics (Rodell et al., 2018). However, the vast majority of process-based and observational studies are concentrated on the Ganga–Brahmaputra–Meghna (GBM) Delta and its Bengal Basin continuation (Shamsudduha et al., 2022). The East Ganga Plains (EGP), and in particular the Kosi–Gandak interfan, the zone between two of the most sediment-laden Himalayan tributaries and the single most wetland-rich part of the non-deltaic Ganga Plains (Singh & Sinha, 2020), remain comparatively underrepresented in the global literature despite hosting millions of people and exhibiting some of the most pronounced hydrological stresses in the IGP (Singh et al., 2017).

Despite persistent monsoon floods, wetlands and small groundwater-fed tributaries across the EGP are increasingly drying, threatening biodiversity, livelihoods, and groundwater-dependent agriculture. Previous work has documented flood risks, wetland loss, and groundwater decline individually (Rodell et al., 2009; Singh & Sinha, 2021; Singh et al., 2017), but these studies remain geographically and thematically fragmented. The most influential regional-scale evidence, namely GRACE-based groundwater depletion (Rodell et al., 2009), irrigation-driven greening (Rodell et al., 2018), and surface-water change (Nagel et al., 2025), addresses either the entire IGP as a single unit or focuses on the GBM Delta and its Bangladesh continuation (Shamsudduha et al., 2022). At these spatial scales, the EGP signal is diluted within the broader IGP average or simply absent from delta-focused analyses. No prior study has synthesised multi-proxy observational evidence into a unified hydrological framework specifically for the EGP, nor tested whether the basin-scale GRACE and optical remote sensing signals are coherent at the interfan scale where the paradox is most acute.

Using Gravity Recovery and Climate Experiment (GRACE) gravimetry (Rodell et al., 2009), Height Above Nearest Drainage (HAND) (Nobre et al., 2011), Copernicus DEM-based topography, Landsat-derived Modified Normalized Difference Water Index (MNDWI) (Xu, 2006), and NDVI time-series across the EGP, we document a basin-scale paradox: flood surpluses in embanked rivers coexist with drying of wetlands and small tributaries, even as irrigation-driven greening masks the underlying water stress. The Kosi–Gandak interfan, which hosts the highest density of floodplain wetlands in the non-deltaic plains (Singh & Sinha, 2020), provides the most spatially coherent signal and is therefore the focus of detailed HAND and sub-regional wetness trend analysis. Three features distinguish this study from antecedent work on the IGP: (a) the EGP-wide geographic framing, with the interfan as its wetland epicentre, going beyond individual-site or delta-focused studies; (b) the integration of five complementary satellite-derived proxies into a unified connectivity framework; and (c) the explicit GLDAS-based groundwater component validation, confirming that the GRACE signal at the interfan scale is overwhelmingly a groundwater signal.

2. Study area and methods

The EGP spans the north Bihar and eastern Uttar Pradesh lowlands, an extremely low-gradient alluvial tract built by Himalayan tributaries of the Ganga. Historically, monsoon floods recharged floodplain wetlands and shallow aquifers through lateral spill and seasonal inundation. The study area spans 85.20–86.35°E and 25.15–26.00°N. The Kosi–Gandak interfan contains the highest density of floodplain wetlands in the non-deltaic plains and therefore provides the clearest setting in which to test whether present-day drying reflects topographic position or hydrological disconnection (Singh & Sinha, 2020). Since the 1950s, embankment construction in Bihar has expanded from about 160 km to more than 3400 km, fundamentally altering surface-water routing and sedimentation patterns (Sahani et al., 2023).

We used Landsat surface-reflectance data for 1988–2022 to derive annual and seasonal MNDWI and NDVI, Terra-MODIS scenes for synoptic land-cover context, the LGRIP30 irrigation product for cropland extent, Copernicus DEM and Height Above Nearest Drainage (HAND) for topographic connectivity, GRACE and GRACE-FO mascon data for terrestrial water storage, GLDAS Noah 2.1 components for water-storage partitioning, IMD rainfall for monsoon forcing and Dartmouth Flood Observatory records for flood magnitude (Brakenridge et al., 2024). Embankments were digitised from Survey of India toposheets and verified against Google Earth imagery. Full data sources, detailed methodology, code and sensitivity analyses are provided in the Supplementary Information and linked repository.

Groundwater storage anomaly was estimated using the standard GRACE residual approach, subtracting GLDAS soil moisture, canopy water, snow water equivalent and a JRC-derived surface-water term from total terrestrial water storage (Rodell et al., 2009; Pekel et al., 2016; Getirana et al., 2025). To isolate genuine wetlands from perennial channels and actively inundating floodplain belts, we applied a Landsat trajectory classification to annual MNDWI and retained only diminishing, lost and intermittent wetness classes following Singh and Sinha (2022) using open-source software `WetlandMapper` (Singh, 2026). We then quantified HAND (Nobre et al., 2011) distributions for these wetland pixels and tested cross-variable annual correlations among groundwater storage, wetland MNDWI and NDVI. The emphasis is on coherence of direction, persistence and spatial concentration rather than on any single metric alone.

3. Results and discussion

3.1 Flood-rich channels, flood-poor floodplains

Across the East Ganga Plains, decades of levee and embankment construction have confined monsoon flows to narrow corridors (Kumar et al., 2014), amplifying in-channel flood stages while depriving adjoining floodplains of seasonal inundation (Fig. 1). Historical flood assessments in Bihar show that despite dramatic embankment expansion since the 1960s, flood-prone area and risk have *increased* (Fig. 1A, B, G), partly due to aggradation and reduced conveyance within the confined belt (Sahani et al., 2023; Sinha et al., 2013; Sinha et al., 2019). Embankment breach histories on the Kosi further illustrate the fragility of hard defences under high sediment loads and low gradients (Sinha et al., 2019). In short, structural flood control has externalised water away from floodplains during ordinary monsoons, yet intensified disaster potential during extremes: an archetypal case of risk shifting rather than risk reduction.

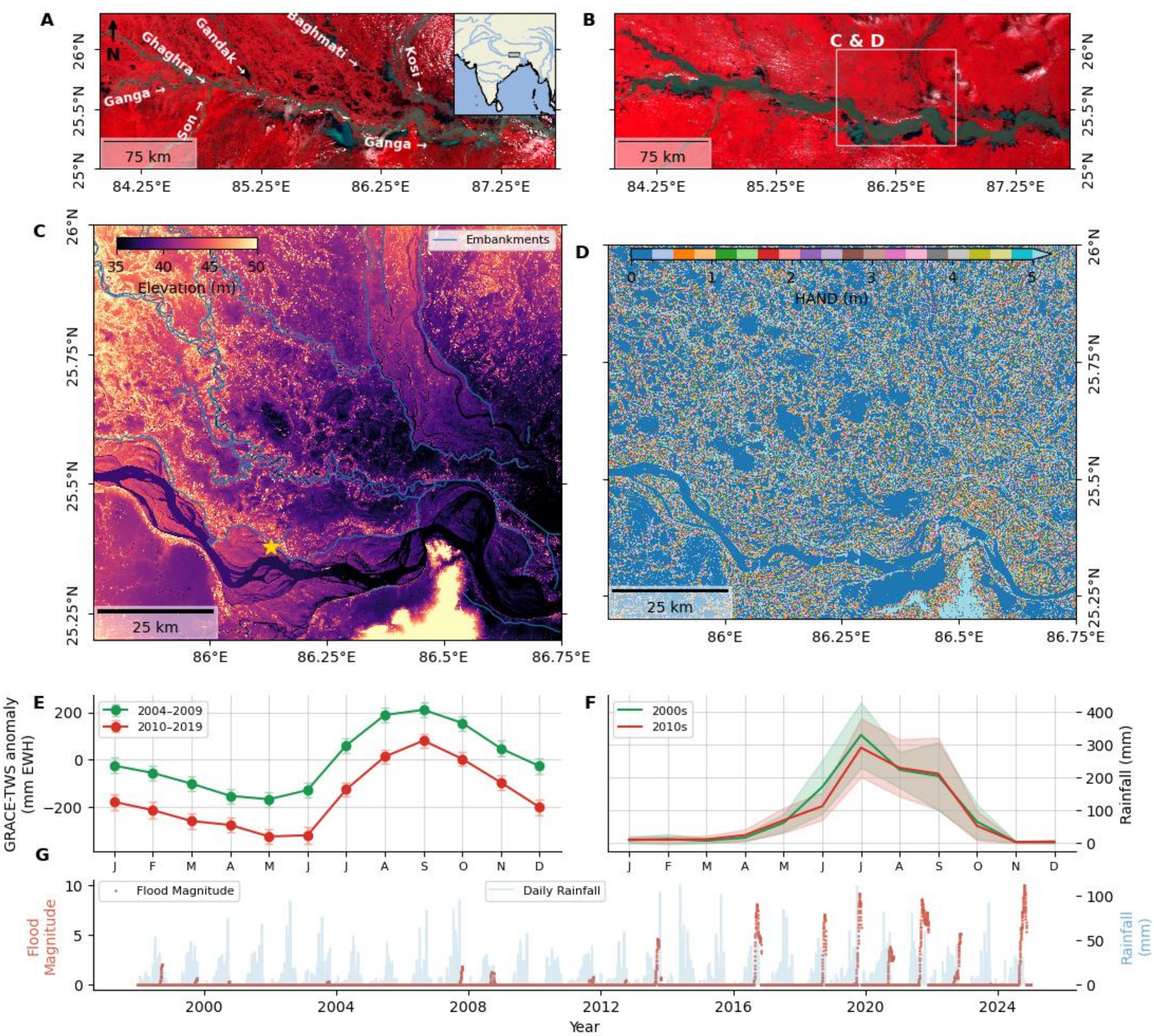

Fig. 1. Study area and observational context of the East Ganga Plains (EGP) hydrological paradox. (A) Terra-MODIS false-colour composite (bands 2-1-4; NIR-Red-Green) for September 2000, showing the EGP at peak monsoon inundation. (B) Same composite for September 2024, illustrating the reduction in surface water extent and increase in agricultural cover over the study period. Inset: location of the study area within India; the rectangle marks the EGP domain. (C) Copernicus DEM (GLO-30) of the Kosi–Gandak interfan, with embankments shown in blue; the gold star marks the Bhagwanpur sub-region. (D) Height Above Nearest Drainage for the same extent, illustrating the extremely low relief of the floodplain system. (E) Monthly GRACE-TWS anomaly (mm EWH) and decadal climatologies for the 2004–2009 and 2010–2019 epochs, showing the shift toward persistent negative storage anomalies. (F) Monthly IMD rainfall climatology for the same two epochs, confirming stationary monsoon forcing. (G) Daily IMD rainfall (blue) and Ganga flood-magnitude record (Dartmouth Flood Observatory; red) for 1998–2024, illustrating increasing flood magnitude under stable rainfall.

3.2 Wetlands under sustained hydrological stress

Geomorphically, all wetlands in the EGP are riverine wetlands (Singh & Sinha, 2020) that depend on hydrological connectivity with rivers for their functioning (Singh et al., 2021). In the absence of anthropogenic modification, these wetlands would receive water during high monsoon flows, dampening floods and recharging groundwater through slow downstream release. In the present scenario, floodplains have been stressed, natural hydrological regimes altered, and wetlands are being converted to agriculture (Singh & Sinha, 2021). Time-series analysis of wetlands across the EGP shows significant water-cover contraction (negative MNDWI trends, $p < 0.05$) over the past few decades (Fig. 2). Embankments have disconnected rivers from their floodplains (Singh et al., 2021), preventing overbank flows that would normally recharge wetlands (Fig. 1C). HAND analysis of the 13,439 trajectory-classified wetland pixels (Supplementary Information) reveals that, after excluding pixels classified as perennial channels ($n = 666$) and as new or intensifying floodplain water ($n = 4{,}370$), the median HAND of genuine wetland bodies remains 0.00 m, with an interquartile range of 0.00–0.30 m. Fully 73.3% of wetland pixels lie within 0.25 m of their nearest drainage thalweg, 86.9% within 1.00 m, and 92.6% within 2.00 m (Figs 1D and S1C). A median of zero, after river pixels have been removed, means that the typical wetland body occurs at the same elevation as the channel it adjoins, and would receive water under virtually any pre-embankment overbank flow. The fact that these wetlands are desiccating despite this topographic proximity is unambiguous evidence that embankments, not natural relief, impose the hydrological isolation (Singh et al., 2017). Notably, this analysis is performed on the modern DEM, which already incorporates post-embankment channel aggradation inside the leveed belt (Section 3.7). True pre-embankment HAND values would have been even lower, making these results conservative with respect to historical connectivity potential.

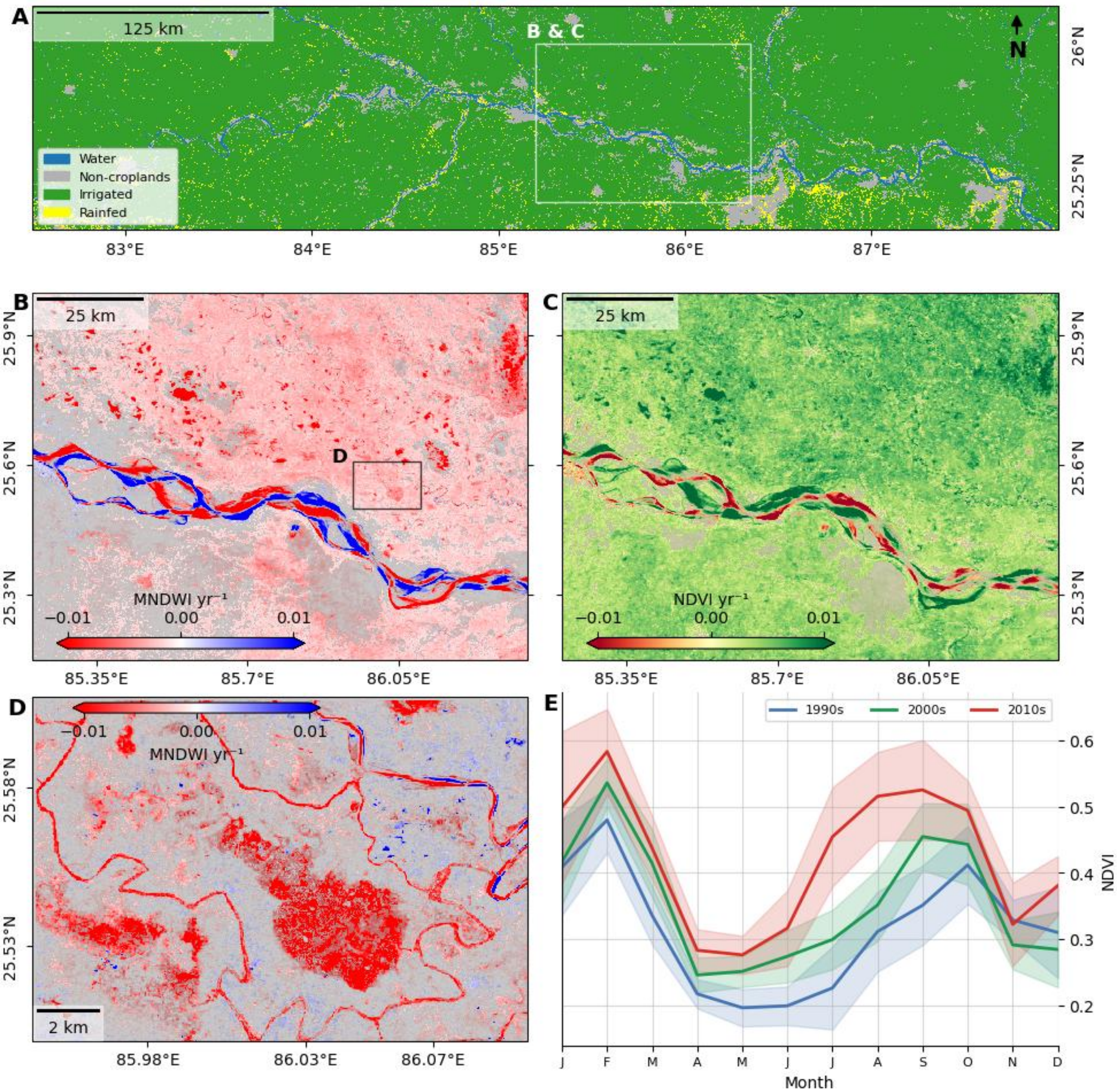

Fig. 2. Remote sensing evidence for irrigation-driven landscape change across the EGP. (A) Irrigated cropland extent (LGRIP30, 2015), showing dominance of irrigated agriculture across the EGP. (B) Annual MNDWI trend (1988–2022) across the Kosi–Gandak interfan; negative values (brown) indicate significant water-cover loss ($p < 0.05$); stippling indicates non-significant pixels. (C) Annual NDVI trend over the same extent; positive values (green) indicate significant vegetation greening. (D) Post-monsoon (September–November) MNDWI trend in the Bhagwanpur sub-region, showing spatially concentrated drying of groundwater-fed streams and wetlands. (E) Monthly NDVI climatology for three epochs (1990s, 2000s, 2010s), showing progressive greening consistent with irrigation intensification rather than increased rainfall.

3.3 Small rivers and tributary desiccation

Remote sensing records reveal seasonal drying, shrinking, and greening of small streams and tributaries, particularly those fed by groundwater (Fig. 2D). The post-monsoon MNDWI trend (September–November) in the Bhagwanpur sub-region, which is dominated by groundwater-fed streams and wetlands, shows statistically significant drying that is spatially concentrated on small streams and wetlands (Fig. 2D). GRACE-TWS data confirm a basin-wide decline in groundwater storage over the same period (Fig. 3), consistent with reduced aquifer levels diminishing baseflows. These findings extend the paradox: not only wetlands, but also the small tributaries that depend on groundwater, are drying under conditions of stable rainfall and increasing flood frequency in the main channels.

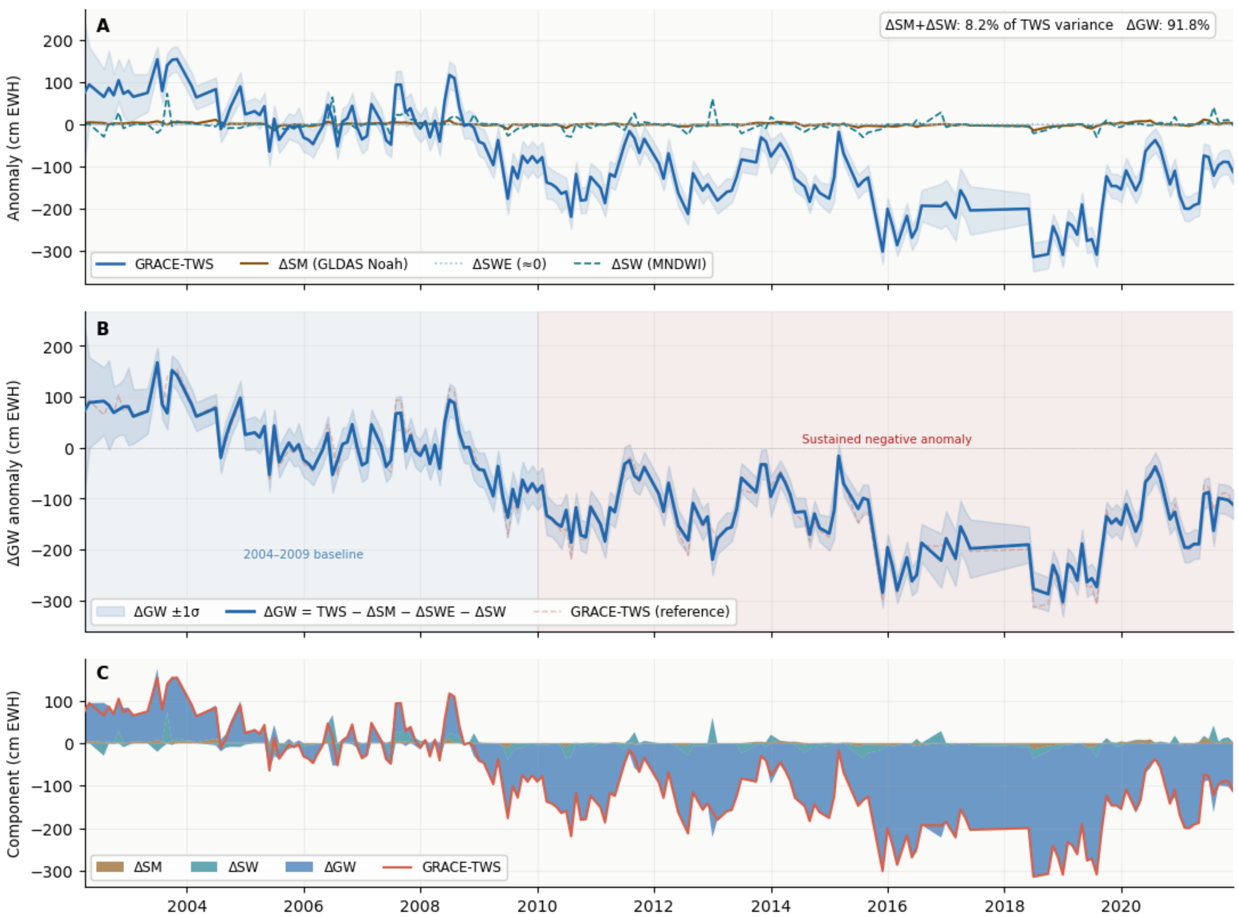

Fig. 3. GRACE-TWS component separation using GLDAS Noah 0.25° (see Supplementary Information). (A) Monthly time series of all components (GRACE-TWS, ΔSM, ΔSWE, ΔSW) as anomalies in cm EWH relative to the 2004–2009 baseline. Grey shading shows ±1σ GRACE uncertainty. (B) Isolated ΔGW anomaly (= TWS − ΔSM − ΔSWE − ΔSW); blue shading = 2004–2009 baseline epoch; red shading = post-2010 period of sustained negative anomaly. (C) Stacked component decomposition showing the dominance of ΔGW in total TWS variance.

3.4 Groundwater storage decline

GLDAS Noah component separation confirms that ΔGW dominates the GRACE-TWS signal in the EGP: the variance ratio Var(ΔGW)/Var(TWS) is 91.8%, while the corresponding ratios for the individual non-groundwater components are all negligible (ΔSM: 0.1%; ΔSWE: 0.0%; ΔSW: 1.6%). These ratios do not sum to 100% because variance is not additive in the presence of cross-covariance terms; the residual reflects correlations among components rather than any unaccounted signal. The GLDAS subtraction changes the inferred multi-decadal ΔGW anomaly by less than 1% relative to raw GRACE-TWS, validating the use of GRACE-TWS as an effective groundwater proxy in this irrigated setting. Snow water equivalent is negligible (0.0%), consistent with the warm Ganga plains setting.

The ΔGW record shows a sustained negative departure from the 2004–2009 baseline throughout the 2010s and 2020s (Fig. 3B), consistent with the decadal aquifer depletion signal. The departure is progressive: early GRACE years (2002–2009) cluster near the baseline, whereas the 2010–2022 period is characterised by persistently negative anomalies reaching tens of centimetres EWH below baseline. The direction and persistence of the anomaly are unambiguous; however, its absolute magnitude at this scale requires piezometric cross-validation.

A critical test of whether the ΔGW decline is climatically forced or anthropogenically driven is provided by the temporal relationship between ΔGW and monsoon rainfall. Standardised z-score anomalies show that ΔGW has been persistently negative throughout the post-2009 period (Fig. S2B), whereas annual rainfall z-scores remain around zero with no secular trend (Fig. S2C). This asymmetry, a unidirectional groundwater decline against stationary rainfall variability, rules out precipitation deficit as the primary driver and is consistent with a progressive increase in groundwater abstraction for irrigation. The temporal divergence between a non-trending rainfall signal and a persistently declining groundwater record is among the clearest lines of evidence distinguishing anthropogenic depletion from natural climatic forcing in the EGP.

3.5 Irrigation-driven greening amid water scarcity

Irrigated agriculture dominates land use in these plains (Fig. 2A) (Teluguntla et al., 2023). Analysis of NDVI trends shows significant increases in vegetation greenness across the plains (Fig. 2C, E), despite stable rainfall (Figs. 1F, G). This greening corresponds to irrigation expansion supported by increased groundwater abstraction (Fig. 3). The anti-correlated temporal trajectories of GRACE-TWS and NDVI (declining storage against rising greenness) are consistent with, though not conclusive proof of, a causal link between irrigation intensification and groundwater depletion. While crops appear productive, the underlying aquifer decline exacerbates the paradox: surface floods persist in the main channels, yet groundwater-fed tributaries and wetlands are hydrologically stressed.

3.6 Multi-proxy signal coherence

All three cross-variable correlations (n = 20 annual observations) are significant and fall in the direction predicted by the connectivity-loss hypothesis ($p \leq 0.004$; Fig. 4). Each correlation is considered in turn below, before the coupling is resolved by topographic position through HAND-class stratification (Fig. 5).

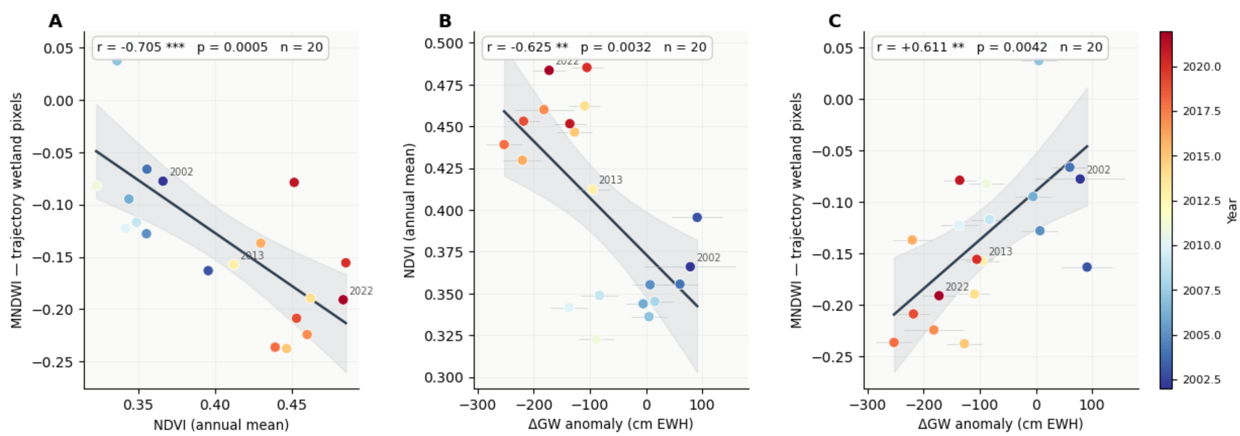

Fig. 4. Cross-variable Pearson correlations between annual mean ΔGW, MNDWI (trajectory-classified wetland pixels only), and NDVI (n = 20 annual observations). Points are coloured by year (blue = early, red = recent). Grey shading shows 95% confidence band on the regression. Uncertainty bars on ΔGW reflect propagated mascon uncertainty. (A) NDVI versus MNDWI ($r = -0.705$, $p < 0.001$); this pair is independent of GRACE gravimetry and is derived entirely from Landsat spectral bands. (B) ΔGW versus NDVI ($r = -0.625$, $p = 0.003$). (C) ΔGW versus MNDWI ($r = +0.611$, $p = 0.004$). All three correlations are in the direction predicted by the connectivity-loss hypothesis; the probability that all three fall in the predicted direction by chance is 12.5%.

NDVI versus MNDWI ($r = -0.705$, $p < 0.001$). The strongest result and the one entirely independent of GRACE: as vegetation greenness increases, surface wetland water cover decreases. Both signals are derived from independent Landsat bands, and neither involves gravimetric data or any model output. This anti-correlation, sustained across three decades of observation, is the clearest fingerprint of water reallocation from wetlands into irrigated crops.

ΔGW versus NDVI ($r = -0.625$, $p = 0.003$). As isolated groundwater storage declines, vegetation greenness increases, consistent with sustained abstraction for irrigation driving both signals simultaneously. Using raw TWS in place of ΔGW yields $r = -0.624$ ($p = 0.003$), confirming that the SM subtraction does not materially alter the result.

ΔGW versus MNDWI (r = +0.611, p = 0.004). Declining groundwater storage co-varies significantly with declining wetland water cover, measured over wetland pixels only after trajectory-based exclusion of river channels and active floodplains. The raw TWS equivalent is r = +0.630 (p = 0.003), again demonstrating that the GLDAS subtraction does not change the conclusion: the GRACE signal in the EGP is already effectively a groundwater signal.

We additionally tested whether the ΔGW–MNDWI coupling varies systematically with HAND class (Fig. 5). The correlation is statistically significant in the two lowest-lying classes: 0–0.10 m (r = +0.664, p = 0.001) and 0.10–0.25 m (r = +0.458, p = 0.042). The three higher classes yield positive but non-significant correlations: 0.25–0.50 m (r = +0.387, p = 0.092), 0.50–1.00 m (r = +0.340, p = 0.143), and > 1.00 m (r = +0.399, p = 0.081). Together, the two significant HAND classes encompass 9,848 wetland pixels (73.3% of the total), all lying within 0.25 m of their nearest drainage thalweg, exactly the pixels in closest topographic contact with the drainage system prior to embankment construction. The concentration of significant coupling in these lowest-lying classes is consistent with direct surface connectivity as the primary pathway: wetlands topographically equivalent to their adjoining channels show the strongest and most demonstrable co-variation with groundwater decline. The positive but non-significant correlations in the higher HAND classes indicate that the drying signal extends into less-connected parts of the wetland population, consistent with the broader groundwater drawdown suggested by the GRACE record, but these effects are not statistically demonstrable at n = 20 annual observations. The HAND-stratified pattern thus reinforces the central finding: embankment-imposed topographic disconnection, concentrated in the HAND ≤ 0.25 m population, is the dominant and statistically supported coupling mechanism.

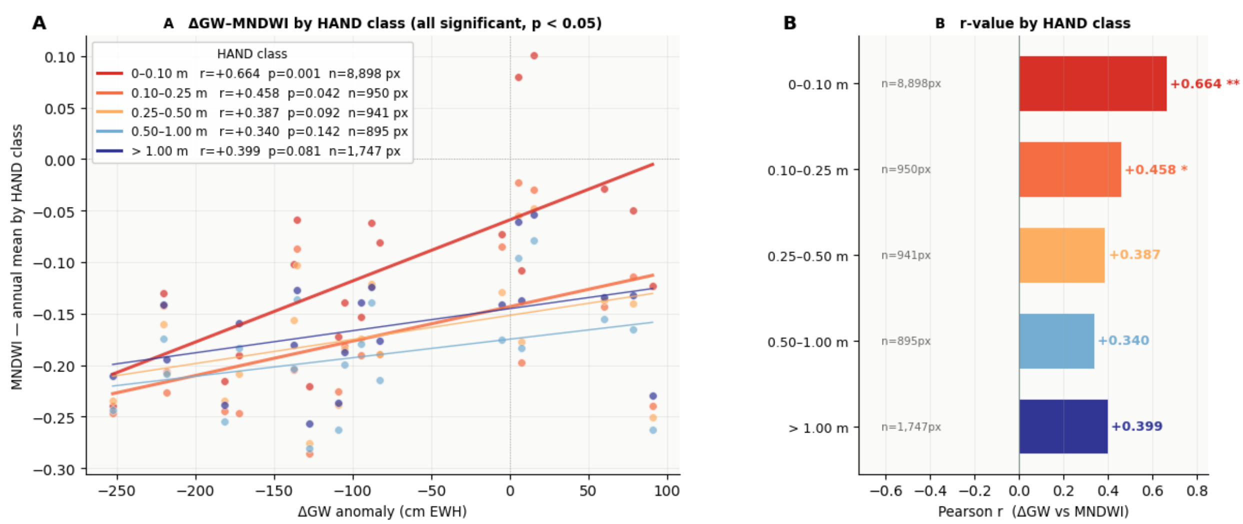

Fig. 5. ΔGW–MNDWI correlation stratified by HAND class, using trajectory-classified wetland pixels (Supplementary Information). (A) Scatter plots and regression lines for each HAND class; line weight reflects statistical significance (bold = $p < 0.05$). (B) Pearson r-values by HAND class; the two lowest-lying

classes (HAND ≤ 0.25 m, encompassing almost three-quarters of all wetland pixels) are statistically significant; higher classes yield positive but non-significant correlations.

The probability of all three aggregate correlations falling in the predicted direction by chance is $(0.5)^3 = 12.5\%$; and all three are significant at $p < 0.01$, which makes the joint evidence substantially stronger. The spatial stratification by HAND and the temporal coherence of five independent proxies collectively provide a strong observational basis for the proposed connectivity-loss mechanism. The temporal decoupling between stationary rainfall and persistently declining ΔGW (Section 3.4; Fig. S2) further eliminates reduced precipitation as a competing explanation, leaving anthropogenic water redistribution, that is, embankment-driven floodplain disconnection combined with groundwater abstraction for irrigation, as the most plausible explanation consistent with all lines of evidence.

The novelty of this study lies not in the individual proxies (GRACE, NDVI, and MNDWI have all been applied across the broader IGP) but in their first combined application at the EGP scale with explicit groundwater validation, where the paradox of coexisting floods and desiccation is most acute and strongly linked to embankment-driven connectivity loss.

3.7 Sediment maldistribution inside the leveed belt

Sediment dynamics further amplify the paradox. Leveed corridors promote in-channel deposition, raising bed elevations and water surfaces for any given discharge, while wetlands and floodplains, starved of overbank silt, lose both elevation capital and nutrient inputs (Fig. 1C). The DEM analysis shows that riverbeds inside embankments now stand above adjacent floodplain surfaces, a reversal of natural morphology. The net effect of confinement is a *maldistribution* of sediment: accumulation in the thalweg and behind embankments, and deficit on the floodplains (Sinha et al., 2019).

3.8 The coupling that matters: a connectivity framework

The basin exhibits *dual water stress*: flood surpluses during the monsoon coexisting with baseflow deficits in summer, mediated by human restructuring of water storage pathways. Within a connectivity framework (Singh et al., 2021), embankments and managed infrastructure force more water and sediment to remain *in-channel* when floodplain ecosystems and aquifers need periodic *out-of-channel* lateral exchanges. Simultaneously, groundwater pumping extracts storage from the floodplain water balance. Without restoring optimal connectivity, both temporally (when) and spatially (where), measures aimed solely at flood control (higher levees) or solely at scarcity (deeper wells) will intensify the other half of the problem. Restoring controlled river–floodplain connectivity would: (a) reduce in-channel flood hazard; (b) replenish groundwater through floodplain recharge; (c) sustain baseflows in downstream small tributaries.

3.9 Research priorities and monitoring framework

Resolving the EGP hydrological paradox requires both filling critical knowledge gaps and building the observational infrastructure to detect change. We identify four research priorities and a complementary monitoring framework, ordered from investigative questions to practical implementation.

Research priorities: (a) **reconnection thresholds:** determine the minimum overbank flows required to sustain wetlands and groundwater-fed tributaries, accounting for embankment geometry and channel aggradation; (b) **piezometric validation of ΔGW magnitude**: GLDAS Noah component separation confirms that GRACE-TWS is overwhelmingly a groundwater signal in the EGP (91.8% of variance), so the next priority is to cross-validate the inferred depletion rate with in-situ piezometer data at the interfan scale, and to quantify how much of the depletion is attributable to reduced floodplain recharge versus increased abstraction for irrigation; (c) **sediment–hydrology feedbacks**: quantify how channel aggradation inside the leveed belt affects the floodplain water balance, and whether levee-induced bed elevation differences between embanked and unembanked reaches now exceed HAND-implied connectivity thresholds; (d) **adaptive infrastructure trials**: test pilot-scale interventions such as controlled levee openings, managed aquifer recharge, and seasonal flood routing into floodplains, measuring hydrological, ecological, and social co-benefits simultaneously.

Progress on these priorities requires a sustained, integrated observational system. We propose the following components: continued GRACE-FO gravimetry with GLDAS-based ΔGW isolation, supplemented by interfan-scale piezometer networks to cross-validate satellite-derived depletion rates and constrain absolute magnitudes; systematic remote sensing of wetland hydroperiods at annual or seasonal resolution (Singh & Sinha, 2021), as new Landsat and Sentinel-2 data accumulate; piezometer networks and isotope or tracer programmes to quantify groundwater–surface-water exchange fluxes and attribute depletion between irrigation abstraction and reduced floodplain recharge; turbidity sensors and sediment gauges deployed both inside and outside embanked zones to measure sediment maldistribution rates and their evolution over time; water-quality surveillance integrating flood pulses, agricultural runoff chemistry, and groundwater composition to assess ecosystem and drinking-water consequences of the paradox.

Underpinning all the above requires a conceptual reorientation: embankments should be reimagined not as rigid barriers but as adjustable systems capable of safe, seasonal reconnection with their floodplains. Flood-to-recharge schemes (routing excess monsoon water into floodplains and wetlands to replenish aquifers) and adaptive levee designs that reduce peak flows while restoring wetland hydroperiods represent the most tractable near-term interventions. The overarching goal is an integrated management system that treats floods, wetlands, and aquifers as one coupled system rather than separate engineering problems.

3.10 Limitations and implications

This interpretation has four main limitations. First, GRACE is best suited to regional aggregation, so the absolute magnitude of groundwater decline at interfan scale should be validated with piezometers. Second, HAND describes topographic potential for connection rather than hydraulic flux directly. Third, the observational evidence supports a parsimonious anthropogenic explanation, but it does not separate the individual contributions of embankments, pumping and other human interventions with a formal attribution model. Fourth, the surface-water term in the GRACE residual assumes a mean water depth of 2 m; because ΔSW accounts for only 1.6% of TWS variance, and because the wetlands concerned are shallower than this, plausible alternative depths change ΔGW negligibly (Supplementary Information). These are real constraints, but they do not remove the central result because the argument rests on convergence among multiple independent datasets rather than on a single proxy.

The management implication is that flood control and water-security planning cannot be treated as separate problems in the EGP or in any floodplain system. Measures that only raise or harden embankments may further reduce recharge and wetland hydroperiods, while measures that only deepen groundwater use intensify dry-season scarcity. The more promising direction is controlled reconnection: targeted floodplain recharge, adaptive embankment operation, piezometric monitoring and continued satellite surveillance of wetland hydroperiods. The findings are relevant beyond the Ganga Plains because they show how heavily managed alluvial plains can appear flood-abundant and water-scarce at the same time when connectivity is re-engineered.

4. Conclusions

The East Ganga Plains exhibit a coherent hydrological paradox: embanked rivers flood, yet nearby wetlands, groundwater-fed tributaries and aquifer storage are declining under stable monsoon rainfall. The paradox is resolved when the basin is viewed through a connectivity framework. Wetlands that are topographically poised to receive overbank recharge are drying, groundwater storage shows a sustained negative anomaly, vegetation greenness rises with irrigation expansion, and all three annual signals co-vary in the direction expected from embankment-driven disconnection plus groundwater abstraction.

This study therefore shifts the interpretation of the EGP from a simple flood-prone landscape to a coupled system experiencing simultaneous channel flood surplus and floodplain water deficit. The central practical implication is that river management, groundwater management and wetland conservation must be designed together. In the absence of controlled reconnection and monitoring, the region is likely to remain trapped in a cycle of rising flood hazard, wetland loss and groundwater depletion.

Acknowledgements

MS is a Royal Society Newton International Fellow at Aberystwyth University and gratefully acknowledges the Royal Society and Aberystwyth University for continued support. We acknowledge NASA, ESA/Copernicus, USGS, IMD Pune and the Dartmouth Flood Observatory for openly accessible datasets used in this study. Claude (Anthropic) and ChatGPT (OpenAI) were used to improve the readability of the accompanying Jupyter Notebook in the Supplementary Information and to copy-edit the manuscript text. The authors reviewed all output and take full responsibility for the content of this paper.

Funding

MS is supported by the Royal Society through a Newton International Fellowship (NIR/R1/232344).

Competing interests

The authors declare no competing interests.

Data availability statement

All datasets used are publicly available. MODIS and GRACE/GRACE-FO data were obtained from NASA Earthdata; GLDAS Noah from NASA GES DISC; Landsat, JRC Global Surface Water and Copernicus GLO-30 from Google Earth Engine; HAND from AWS; rainfall from IMD Pune; flood magnitude from the Dartmouth Flood Observatory; and irrigation extent from LGRIP30. The Google Earth Engine script and Jupyter workflow are available at https://github.com/manudeo/Hydrological_Paradox_Ganga_Plains and in the Supplementary Information.

References

Brakenridge, G., Kettner, A., Nghiem, S., Kugler, Z., De Groeve, T., Paris, S., & Cohen, S. (2024). River and Reservoir Watch Version 4.6 Satellite-Based River Discharge and Reservoir Area Measurements 1998-Present: Technical Summary. The Flood Observatory River and Reservoir Watch.

Chuphal, S. D., Thirumalai, K., & Mishra, V. (2025). Recent drying of the Ganga River is unprecedented in the last 1,300 years. PNAS, 122(40), e2424613122.

Getirana, A., Kumar, S., & Rodell, M. (2025). Inconsistencies in GRACE-Based Groundwater Storage Estimation: A Call for a Proper Use of Land Surface Models. Geophysical Research Letters, 52, e2025GL119197.

Kumar, R., Jain, V., Babu, G. P., & Sinha, R. (2014). Connectivity structure of the Kosi megafan and role of rail-road transport network. Geomorphology, 227, 73–86.

Nagel, G. W., Darby, S. E., & Leyland, J. (2025). Surface Water Transitions 1984–2022: A Global Dataset at Annual Resolution. Scientific Data, 12, 1729.

Nobre, A. D., Cuartas, L. A., Hodnett, M., Renno, C. D., Rodrigues, G., Silveira, A., & Saleska, S. (2011). Height Above the Nearest Drainage: a hydrologically relevant new terrain model. Journal of Hydrology, 404(1–2), 13–29.

Pekel, J.-F., Cottam, A., Gorelick, N., & Belward, A. S. (2016). High-resolution mapping of global surface water and its long-term changes. Nature, 540(7633), 418–422.

Rodell, M., Velicogna, I., & Famiglietti, J. S. (2009). Satellite-based estimates of groundwater depletion in India. Nature, 460(7258), 999–1002.

Rodell, M. et al. (2018). Emerging trends in global freshwater availability. Nature, 557, 651–659.

Sahani, R. K., Badiger, S., Samrat, A., & Krishnan, S. (2023). Flood frequency and flood intensity changes in the post embankment period in the Kosi sub-basin India. Frontiers in Water, 5, 1017945.

Shamsudduha, M. et al. (2022). The Bengal Water Machine: Quantified freshwater capture in Bangladesh. Science, 377, 1315–1319.

Sharma, C., Dayal, D., & Shukla, A. K. (2025). Drought Risk and Hydrological Changes in the Ganga River Basin, India. Physics and Chemistry of the Earth, Parts A/B/C, 104107.

Singh, M. (2026). WetlandMapper: A Python package for automatic wetland mapping, dynamics classification, and cover-type characterisation. https://doi.org/10.5281/zenodo.18967176

Singh, M., & Sinha, R. (2020). Distribution, diversity, and geomorphic evolution of floodplain wetlands in the Ganga plains of north Bihar, India. Geomorphology, 351, 106960.

Singh, M., & Sinha, R. (2021). Hydrogeomorphic indicators of wetland health inferred from multi-temporal remote sensing data for a new Ramsar site (Kaabar Tal), India. Ecological Indicators, 127, 107739.

Singh, M., & Sinha, R. (2022). A basin-scale inventory and hydrodynamics of floodplain wetlands based on time-series of remote sensing data. Remote Sensing Letters, 13(1), 1–13. https://doi.org/10.1080/2150704X.2021.1980919

Singh, M., Sinha, R., & Tandon, S. K. (2021). Geomorphic connectivity and its application for understanding landscape complexities: a focus on the hydro-geomorphic systems of India. Earth Surface Processes and Landforms, 46(1), 110–130.

Singh, M., Tandon, S. K., & Sinha, R. (2017). Assessment of connectivity in a water-stressed wetland (Kaabar Tal) of Kosi–Gandak interfan, north Bihar Plains, India. Earth Surface Processes and Landforms, 42(13), 1982–1996.

Sinha, R., Gaurav, K., Chandra, S., & Tandon, S. K. (2013). Exploring the channel connectivity structure of the August 2008 avulsion belt of the Kosi River, India. Geology, 41(10), 1099–1102.

Sinha, R., Gupta, A., Mishra, K., Tripathi, S., Nepal, S., Wahid, S., & Swarnkar, S. (2019). Basin-scale hydrology and sediment dynamics of the Kosi river in the Himalayan foreland. Journal of Hydrology, 570, 156–166.

Teluguntla, P., Thenkabail, P., Oliphant, A., Gumma, M., Aneece, I., Foley, D., & McCormick, R. (2023). Landsat-derived global rainfed and irrigated-cropland product 30 m V001. NASA EOSDIS Land Processes DAAC, LGRIP30.001.

Xu, H. (2006). Modification of normalised difference water index (NDWI) to enhance open water features in remotely sensed imagery. International Journal of Remote Sensing, 27(14), 3025–3033.